Symmetry-breaking bifurcations in one-dimensional excitable media

Mark Kness
Center for Nonlinear Dynamics and Department of Physics, University of Texas, Austin, Texas 78712

Laurette S. Tuckerman
Center for Nonlinear Dynamics and Department of Mathematics, University of Texas, Austin, Texas 78712

Dwight Barkley
Program in Applied and Computational Mathematics, Princeton University, Princeton, New Jersey 08544
(Received 6 April 1992)

A two-species reaction-diffusion model is used to study bifurcations in one-dimensional excitable media. Numerical continuation is used to compute branches of traveling waves and periodic steady states, and linear stability analysis is used to determine bifurcations of these solutions. It is shown that the sequence of symmetry-breaking bifurcations which lead from the homogeneous excitable state to stable traveling waves can be understood in terms of an O(2)-symmetric normal form.

PACS number(s): 82.20.Wt, 82.20.Mj, 02.20.+b

I. INTRODUCTION

Wave propagation in homogeneous excitable media implies bistability between states of different spatiotemporal symmetries. Specifically, an excitable medium has a spatially homogeneous steady state: the ground state of the system. This state is linearly stable; however, certain sufficiently large perturbations (beyond an excitability threshold for the medium) do not relax to the homogenous state but instead evolve into propagating waves. Such waves are neither spatially uniform nor time independent, and hence have broken spatiotemporal symmetry with respect to the coexisting homogeneous stable state.

Despite extensive theoretical and experimental study of waves in excitable media (e.g., Refs. 1–18), there has been virtually no focus on the symmetry-breaking bifurcations associated with them. Previous studies have either not explicitly identified symmetry-breaking bifurcations, or have identified the role of symmetry [18], but only for weakly nonlinear state, i.e., states near bifurcations from the homogeneous state. While the weakly nonlinear results are of importance, it cannot be assumed *a priori* that they are applicable to the case of highly nonlinear waves in excitable media.

In this paper we shall examine the sequence of symmetry-breaking bifurcations which connect homogeneous steady states to stable one-dimensional traveling waves in a model excitable medium [19,20]. Our primary purpose is to show that the kind of symmetry-breaking bifurcations which have attracted attention in other physical systems [21–29], particularly those of hydrodynamic origin [30–35], play an important role in dynamics of excitable media.

II. SYMMETRY-BREAKING SCENARIO

Before presenting the model excitable system and its various solutions, we describe a symmetry-breaking scenario which will play a central role in our analysis. This scenario has been observed in a variety of pattern-forming systems having reflectional symmetry and either translational or rotational symmetry [21–35] (see also Refs. [36,37] for a more general discussion). The scenario is most simply captured in the following system of differential equations (normal form):

$$\begin{aligned} \dot{r} &= \mu r - r^3 , \\ \dot{\theta} &= z , \\ \dot{z} &= (r^2 - 1 - z^2) z , \end{aligned} \tag{1}$$

where (r,θ,z) are cylindrical coordinates and μ is a bifurcation parameter. These equations possess several symmetries; that is, there are several transformations which leave the equations invariant. These are

$$R(\alpha):\ \theta \to \theta + \alpha \bmod 2\pi \quad \text{(rotation)} , \tag{2}$$

$$\kappa:\ \theta \to 2\pi - \theta,\quad z \to -z \quad \text{(reflection)} , \tag{3}$$

$$T(\beta):\ t \to t + \beta \quad \text{(time translation)} . \tag{4}$$

When one is interested in time-periodic solutions of the equations, it is common to take the time translations modulo τ, where τ is the period. Then the above transformations constitute a representation of the group $O(2)\times S^1$, where the rotations and reflections represent O(2) and the time translations represent S^1. Solutions of (1) typically break the symmetry of the underlying equations. In particular, the symmetries of solutions will be subgroups of the full group of transformations (2)–(4).

The trivial steady state $r=z=0$ of (1) is left invariant by reflection and all rotations and time translations, that is, it is a fully symmetric state [Fig. 1(a)]. This state is stable for $\mu<0$ and at $\mu=0$ loses stability via what is known as a *circle-pitchfork* (CP) bifurcation. The bifurcating steady state states are given by

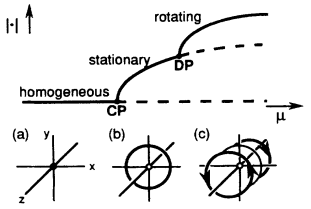

FIG. 1. Illustration of the symmetry-breaking scenario discussed in the text. Shown is a bifurcation diagram together with three representative phase portraits. The bifurcation parameter is μ; the norm is a function which distinguishes different states. CP denotes a circle-pitchfork bifurcation and DP denotes a drift-pitchfork bifurcation. For μ below CP, the origin is stable: phase portrait (a). The branch is labeled homogeneous because the origin is fully symmetric. At CP, a circle of steady states bifurcates from the homogeneous branch and for μ between CP and DP these states are stable: phase portrait (b). At DP the circle of steady states undergoes a drift-pitchfork bifurcation and for μ above DP, there exist two stable counterrotating limit cycles: phase portrait (c).

$$\begin{bmatrix} r \\ \theta \\ z \end{bmatrix} = \begin{bmatrix} \sqrt{\mu} \\ \theta_0 \\ 0 \end{bmatrix}, \tag{5}$$

where θ_0 parametrizes the circle of steady states [Fig. 1(b)]. This bifurcation results in a loss of rotational symmetry for the stable states of the system: the single, rotationally symmetric state ($r=z=0$) bifurcates to a family of states, each of which is not rotationally symmetric, but which transform into one another under rotation. Each of the bifurcating states retains reflection symmetry, however, as do all points which lie in the plane $z=0$. Specifically, steady state (5) is left invariant by the transformation, $R(\theta_0)\circ\kappa\circ R(-\theta_0)$, an element of the group of spatial symmetries (2) and (3) which corresponds to reflection about the line $\theta=\theta_0$. Because states (5) are steady, they are invariant under all time translations. Thus each steady state (5) has the associated symmetry group $Z_2\times S^1$.

At $\mu=1$ there is a secondary bifurcation at which the nontrivial steady states lose stability to two counterrotating limit cycles [Fig. 1(c)]. These limit cycles are given by

$$\begin{bmatrix} r(t) \\ \theta(t) \\ z(t) \end{bmatrix} = \begin{bmatrix} \sqrt{\mu} \\ \theta_0 \pm ct \\ \pm\sqrt{\mu-1} \end{bmatrix}, \tag{6}$$

where $\pm c=\pm\sqrt{\mu-1}$ are the wave speeds of the two limit cycles. Here θ_0 parametrizes the phase of the orbit. This transition to periodic orbits is known as a *drift-pitchfork*, DP, bifurcation because just after the bifurcation, points near the formerly stable circle of steady states begin to drift slowly in one direction or the other. This is very different from a Hopf bifurcation: at the transition, the wave speed is zero and the amplitude of the periodic solutions is finite.

The DP bifurcation breaks the reflectional symmetry of the system. Points on the limit cycles do not have reflection symmetry because they do not lie in the plane $z=0$. Reflection takes points on one periodic orbit to points of the other, counterrotating orbit. In addition, because points on the periodic orbits are not stationary, they are not invariant under time translations. The rotating periodic orbits do, however, maintain a continuous spatiotemporal symmetry: the symmetry of rotating waves. Points on the periodic orbits rotate at constant speed (as they must, due to rotational symmetry), and hence it is possible to compensate for time translations with rotations. Specifically, the transformation $R(-ct)\circ T(t)$, for any t, leaves points on the $z>0$ periodic orbit invariant (and similarly for the $z<0$ orbit). The symmetries of points on the periodic orbits form a one-dimensional subgroup, parametrized by t, of the full symmetries (2)–(4). There are no further bifurcations as μ increases in the normal-form model. Both the CP and DP bifurcations are intimately associated with the symmetries of the system and do not occur in systems without symmetry.

As we shall make explicit shortly, in a one-dimensional excitable medium, homogeneous steady states have the symmetries of the trivial steady state in Fig. 1(a), spatially periodic steady states have the symmetries of the circle of steady states in Fig. 1(b), and periodic traveling waves have the symmetries of the counterrotating limit cycles in Fig. 1(c). Thus the normal form (1) contains the essence of the symmetry breakings leading from homogeneous steady states to traveling waves, with this exception: there is no bistability between states of different symmetries in the normal form. In order to create simultaneously stable states, it is necessary for the solution branches in excitable media to twist and turn, stabilizing and destabilizing via saddle-node bifurcations. After a short description of a model excitable system and numerical methods in the next section, the remainder of the paper will be devoted to exploring the above symmetry-breaking bifurcations in the model system.

III. MODEL AND METHODS

A. Model equations

Our study is based on the following two-species reaction-diffusion model for a one-dimensional (1D) excitable medium [19,20]:

$$\frac{\partial u}{\partial t}=\frac{\partial^2 u}{\partial x^2}+f(u,v), \quad \frac{\partial v}{\partial t}=\frac{\partial^2 v}{\partial x^2}+g(u,v), \tag{7}$$

where the species u and v are functions of x and t. The reaction terms f,g are modeled by

$$f(u,v)=\epsilon^{-1}u(1-u)[u-u_{\rm th}(v)], \tag{8}$$

$$g(u,v)=u-v, \tag{9}$$

with

$$u_{\rm th}(v)=(v+b)/a, \tag{10}$$

where $u_{\rm th}(v)$ is the excitability threshold for the fixed point. Here a,b and ϵ are parameters with $\epsilon\ll 1$ and the physically significant range of u is $0\le u\le 1$ (see Fig. 2

discussed below). We consider here only cases where both species diffuse with the same diffusion coefficient, which is set to unity by choice of length scale.

We rewrite Eqs. (7)–(10) compactly as

$$\frac{\partial \mathbf{u}}{\partial t}=\frac{\partial^2 \mathbf{u}}{\partial x^2}+\mathbf{f}(\mathbf{u}) , \tag{11}$$

where

$$\mathbf{u}(x,t)\equiv\begin{bmatrix} u(x,t) \\ v(x,t) \end{bmatrix}, \quad \mathbf{f}(\mathbf{u})=\begin{bmatrix} f(u,v) \\ g(u,v) \end{bmatrix} .$$

We shall be interested in three classes of solutions to (11): spatially homogeneous steady states, spatially periodic steady states, and periodic traveling waves. Thus we impose periodic boundary conditions

$$\mathbf{u}(x+L,t)=\mathbf{u}(x,t) , \tag{12}$$

where L is the length of the periodic domain.

Steady-state solutions of (11) are given by

$$\mathbf{0}=\frac{\partial^2 \mathbf{u}}{\partial x^2}+\mathbf{f}(\mathbf{u}) , \tag{13}$$

with homogeneous steady states satisfying the algebraic equation

$$\mathbf{0}=\mathbf{f}(\mathbf{u}) . \tag{14}$$

By definition, traveling-wave solutions of (11) are time independent when viewed in a frame traveling at the wave speed c, i.e., after a change of coordinates $x\rightarrow x-ct$. Thus traveling waves satisfy

$$\mathbf{0}=\mathbf{F}(\mathbf{u};c)\equiv\frac{\partial^2 \mathbf{u}}{\partial x^2}+c\frac{\partial \mathbf{u}}{\partial x}+\mathbf{f}(\mathbf{u}) . \tag{15}$$

Solutions to this equation include not only traveling waves, but also homogeneous and periodic steady states as special cases with $c=0$. Hence all the solutions we seek are captured in this single equation.

In addition to finding solutions, $\mathbf{u}$, of Eq. (15), we are interested in determining their stability via linear-stability analysis. Let $\mathbf{DF}(\mathbf{u};c)$ be the linearization of $\mathbf{F}$ about solution $\mathbf{u}$ with wave speed c:

$$\mathbf{DF}(\mathbf{u};c)\equiv\frac{\partial^2}{\partial x^2}+c\frac{\partial}{\partial x}+\mathbf{Df}(\mathbf{u}) , \tag{16}$$

where $\mathbf{Df}(\mathbf{u})$ is the Jacobian of the kinetics $\mathbf{f}(\mathbf{u})$. Then the linear stability problem is written

$$\mathbf{DF}(\mathbf{u};c)\tilde{\mathbf{u}}=\lambda\tilde{\mathbf{u}} , \tag{17}$$

where λ and $\tilde{\mathbf{u}}$ are eigenvalues and eigenvectors. The leading eigenvalues of (17), i.e., the eigenvalues with largest real part, determine the stability of the state $\mathbf{u}$.

Equations (15) and (17) are the equations of interest in this paper. These equations are easily solved analytically for the case of homogeneous steady states. For inhomogeneous steady states and traveling waves we resort to numerical solutions.

B. Numerical methods

To solve (15) numerically, we use standard techniques of numerical analysis and parameter continuation (see, e.g., [38–41]). We discretize the equation on a grid of between $N=256$ and 640 equally spaced points, $x_j=jh$, where the rigid spacing $h=L/N$. Spatial derivatives are approximated by second-order centered differences which incorporate the periodic boundary conditions (12).

After spatial discretization, system (15) consists of $2N$ equations in $2N+1$ unknowns: the function values $(u(x_j),v(x_j))$ and the unknown wave speed c. This indeterminacy results from the symmetries of the problem and is independent of whether or not $c=0$; traveling waves and periodic steady states are determined only up to a spatial phase. To remove the indeterminacy and select one member of the continuum of solutions, we append the phase condition

$$\frac{\partial v}{\partial x}(\bar{x})=0 , \tag{18}$$

where $\bar{x}$ is some selected point.

We use parameter continuation [40,41] to find branches of solutions to (15). For this purpose, we append another equation and unknown to Eqs. (15) and (18). The additional unknown is one of the kinetics parameters, a, of Eq. (10) as will be discussed in Sec. IV A. We then consider solutions to be described by $(\{u(x_j),v(x_j)\},c,a)$, and compute a branch, or curve of solutions, in this $(2N+2)$-dimensional space. The additional equation is provided by the corrector step of the continuation method. Specifically, after computing a predicted solution by adding a multiple of the tangent vector to the curve, we impose the constraint that the difference between predicted and final solutions be perpendicular to this local tangent.

We solve the resulting system of $2N+2$ nonlinear equations by Newton's method. The linear system is pentadiagonal, except for the last four rows and columns (those involving the periodic boundaries; the phase condition and wave speed dependence; and the continuation and parameter dependence) and can be solved efficiently via LU factorization at each Newton step.

After a solution $(\mathbf{u};c)$ to (15) and (18) has been computed, the spatially discretized operator $\mathbf{DF}(\mathbf{u};c)$ of (16) becomes a $2N\times 2N$ matrix, for which Eq. (17) is an eigenvalue problem. We used the algorithm of Sorensen to calculate four leading eigenpairs (eigenvalues and corresponding eigenvectors), for each state of interest. The algorithm, described in detail in Refs. [42,43], uses an amalgamation of the Arnoldi and QR methods (where Q is an orthogonal matrix and R is an upper triangular one) to compute eigenvalues within a desired range, and requires only the action of the matrix on a vector.

Finally, to obtain the initial solution required for continuation, and also to determine the eventual fate of some unstable states, we integrate (11) in time. We use Euler time stepping, with a time step $\Delta t=2h^2/5$ taken smaller than $h^2/2$, the numerical stability limit for a pure diffusion problem. It is not difficult to construct piecewise-constant initial conditions that evolve into

stable traveling waves under time integration. These are then used as a starting point to compute other traveling-wave states, and eventually stationary states.

C. Symmetries

We conclude this section by noting that Eq. (7), or equivalently (15), has precisely the symmetries of the normal-form equations treated in Sec. II. With periodic boundary conditions, translations in x are formally equivalent to rotations, and Eq. (15) has the following symmetries:

$$R(\alpha)\text{: } \mathbf{u}(x,t)\rightarrow\mathbf{u}(x+\alpha \bmod L,t) \text{ (rotation)}, \tag{19}$$

$$\kappa\text{: } \mathbf{u}(x,t)\rightarrow\mathbf{u}(L-x,t) \text{ (reflection)}, \tag{20}$$

$$T(\beta)\text{: } \mathbf{u}(x,t)\rightarrow\mathbf{u}(x,t+\beta), \text{ (time translation)}. \tag{21}$$

Just as for the normal form, the various solutions that we consider in the next section have symmetries which are subgroups of these spatiotemporal symmetries.

There is one additional symmetry of Eq. (15). Consider the transformation $u\rightarrow 1-u$, $v\rightarrow 1-v$ applied to the kinetics (8)–(10):

$$f(1-u,1-v)=-\epsilon^{-1}u(1-u)\times\left[u-u_{\rm th}(v)+\frac{1+2b-a}{a}\right],$$

$$g(1-u,1-v)=-g(u,v).$$

Hence, when the parameters satisfy $a=1+2b$, the kinetics, like the diffusion, transform antisymmetrically, and Eq. (15) has an additional symmetry: $\mathbf{F}(1-\mathbf{u};c)=-\mathbf{F}(\mathbf{u};c)$. While this symmetry in the reaction terms cannot be expected in realistic systems, this symmetry is found in other models currently studied [44].

IV. RESULTS

We now present bifurcation diagrams for three classes of solutions to (15): spatially homogeneous steady states (HSS), spatially periodic steady states (PSS), and periodic traveling waves (TW). We shall emphasize the symmetries of the solutions and their relationship to the normal-form solutions in Sec. II.

A. Homogeneous steady states

Written in component form, Eq. (14) for the homogeneous steady states is

$$0=f(u,v)=\epsilon^{-1}u(1-u)[u-(v+b)/a], \tag{22}$$

$$0=g(u,v)=u-v. \tag{23}$$

The HSS solutions immediately follow:

$$u=v=0, \tag{24}$$

$$u=v=1, \tag{25}$$

$$u=v=\frac{b}{a-1}. \tag{26}$$

We shall refer to these as the zero, one, and middle branches, respectively.

Because the HSS's are independent of x and t, they are invariant under all symmetry operations (19)–(21) and thus correspond to the point $r=z=0$ in the normal form.

It is useful to consider briefly the organization of homogeneous steady states in the (a,b) parameter plane. Shown in Fig. 2 is the parameter plane with representative nullcline diagrams as insets. The u nullcline is the curve on which $\dot{u}=f(u,v)=0$, and the v nullcline is the curve on which $\dot{v}=g(u,v)=0$. The u nullcline consists of the three lines $u=0$, $u=1$, and $u=u_{\rm th}(v)=(v+b)/a$. Only the solid portion of the u nullcline, forming a backwards N, is physically significant for the model kinetics [45]. The v nullcline is $v=u$. At (u,v) points where the u and v nullclines intersect, the system has a HSS.

There are four regions in Fig. 2, distinguished according to the intersection of the v nullcline with the *solid* branches of the u nullcline. In region I the v nullcline intersects only the zero branch of the u nullcline. In region II the v nullcline intersects all three branches. In region III the v nullcline intersects only the one branch of the u nullcline and in region IV it intersects only the middle branch. Throughout most of region IV there are no stable steady states and the homogeneous system is oscillatory (see below). Note that the diagram is symmetric under the transformation $b\rightarrow a-b-1$, as follows from the symmetry of the kinetics discussed in Sec. III C. The four-region diagram shown in Fig. 2 is known as a cross-shaped diagram in the chemical-dynamics literature [46].

The stability of homogeneous solutions is easily found analytically. For a periodic domain of length L, the eigenmodes are trigonometric functions of $2\pi kx/L$ with

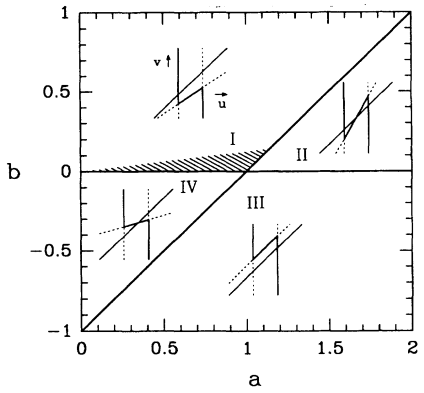

FIG. 2. Phase diagram for the homogeneous states of the system. The diagram is divided into four regions with representative nullcline diagrams in each. Only the solid backwards N-shaped parts of the u nullclines are physically relevant. In region I only the zero branch is stable. In region II the system is bistable. In region III only the one branch is stable. Throughout most of the region IV there are no stable steady states and the homogeneous system is oscillatory. The diagram is symmetric under the transformation $b\rightarrow a-b-1$. Hatching illustrates the portion of region I in which the zero branch is excitable. A symmetrically located portion of region III exists for which the one branch is excitable.

k integer. Substituting

$$\mathbf{u}+\tilde{\mathbf{u}}_0\exp(\lambda t)\times\begin{Bmatrix}\sin\\ \cos\end{Bmatrix}(2\pi kx/L)$$

into Eq. (11), with $\mathbf{u}$ any of (24), (25), and (26), and linearizing, we obtain

$$\begin{bmatrix} f_u-(2\pi k/L)^2 & f_v \\ 1 & -1-(2\pi k/L)^2 \end{bmatrix}\begin{bmatrix}\tilde{u}_0\\ \tilde{v}_0\end{bmatrix}=\lambda\begin{bmatrix}\tilde{u}_0\\ \tilde{v}_0\end{bmatrix},$$

where

$$f_u=\epsilon^{-1}\{(1-u)[u-u_{\rm th}(v)] -u[u-u_{\rm th}(v)]+u(1-u)\}\ , \tag{27}$$

$$f_v=-\epsilon^{-1}u(1-u)/a\ . \tag{28}$$

The eigenvalues are

$$\lambda_{0\pm}=\tfrac{1}{2}\{f_u-1\pm[(f_u-1)^2+4(f_u+f_v)]^{1/2}\}\ , \tag{29}$$

$$\lambda_{k\pm}=\lambda_{0\pm}-(2\pi k/L)^2,\quad k=1,2,\ldots\ , \tag{30}$$

with corresponding eigenvectors

$$\begin{bmatrix}\tilde{u}_0\\ \tilde{v}_0\end{bmatrix}=\begin{bmatrix}1+\lambda_{k\pm}\\ 1\end{bmatrix}.$$

From (30), it is clear that if a HSS is stable to homogeneous ($k=0$) perturbations, then it is also stable to perturbations with any k. Hence, to determine whether a branch is stable, we need only consider the eigenvalues $\lambda_{0\pm}$ corresponding to $k=0$.

The stability of the zero and one branches is immediately found by noting that (28) implies $f_v=0$ for $u=0$ or $u=1$. Equation (29) then simplifies to $\lambda_{0+}=f_u$, $\lambda_{0-}=-1$. For the zero branch, $f_v=-\epsilon^{-1}b/a$, which is negative for positive a and b, and hence the zero branch is stable in regions I and II. For the one branch, we have $\lambda_{0+}=f_u=\epsilon^{-1}[-1+(1+b)/a]$. Thus the one branch is stable for $1+b<a$, i.e., in regions II and III.

The eigenvalues of the middle branch require more algebra to compute, but it is not difficult to verify the following. In Region II (where the zero and one branches are both stable) the middle branch has $\lambda_{0+}>0$ and hence is unstable. Along the curves $b=\frac{1}{2}(a-1)[1\pm\sqrt{1-4\epsilon}]$ in region IV, the middle branch undergoes a homogeneous Hopf bifurcation.

In region I when b is small, the zero-state is a stable but excitable steady state. That is, an initial condition sufficiently perturbed from the zero state returns to it, but only after a substantial excursion. This can be verified by direct simulation of the homogeneous system. However, the definition of excitability is not exact (e.g., Ref. [1], p. 184) and it is not possible to say precisely when the system is excitable. The hatched area in Fig. 2 illustrates *approximately* the parameter regime for which the zero state can be considered excitable. A symmetrically located portion of region III exists in which the one state is excitable. In bistable region II, large perturbations of the zero state lead to the one state rather than returning to the zero state (and vice versa).

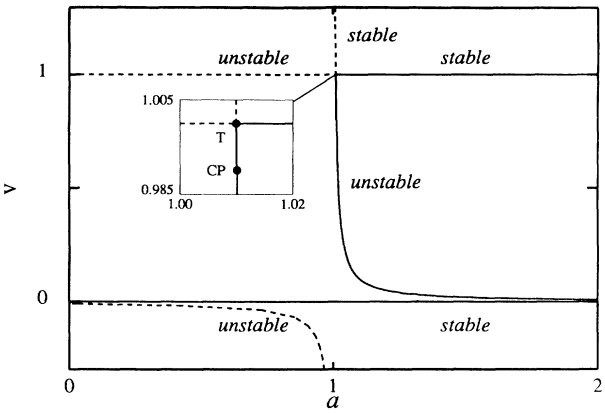

FIG. 3. Bifurcation diagram for homogeneous steady states. The value u is plotted as a function of a along the zero branch, $u=v=0$, the one branch, $u=v=1$, and the middle branch, $u=v=b/(a-1)$. Solid (dashed) curves indicate the physically relevant (irrelevant) states. The middle branch intersects the one branch in a transcritical bifurcation, T, at $a=1+b=1.01$ and undergoes $k=1$ circle-pitchfork bifurcations, CP, at $a=1.0101$ and $a=17.71$ (not shown).

We are primarily interested in the excitable portion of region I. However, to obtain a coherent bifurcation picture, it is also necessary to consider bifurcations occurring in region II. We choose a as the bifurcation parameter and show diagrams for a in the range $0<a<2$ with b fixed at 0.01. The other parameters are also fixed for the remainder of the paper: $\epsilon=\frac{1}{150}$, and $L=21.58$.

Figure 3 shows a bifurcation diagram for the HSS solutions. The zero branch is stable throughout. The one branch becomes stable at $a=1+b$ in a transcritical bifurcation with the middle branch [47]. This bifurcation marks the boundary between regions I and II of Fig. 2.

The eigenvalue λ_{0+} of the middle branch, calculated from formula (29), is plotted on Fig. 4 as a function of a. When $\lambda_{0+}=(2\pi k/L)^2$, the middle branch becomes unstable to modes with wave number $(2\pi k/L)$. In particular, $\lambda_{0+}=(2\pi/L)^2$ at $a=1.0101$ and again at $a=17.715$ (not shown). At these values of a, the middle branch becomes unstable to $k=1$ modes. These instabilities are circle-pitchfork bifurcations through which the periodic steady-state branch is created and eventually destroyed. It can be seen from Fig. 4 that the middle branch is unstable to a considerable number of higher wave-number perturbations which shall not be considered here.

B. Periodic steady states

Figure 5 shows a bifurcation diagram for the periodic steady states which bifurcate from the HSS middle branch. The norm we use to characterize the PSS branch is the spatial average $\langle v\rangle\equiv(1/L)\int_0^L v\,dx$. Representative spatial profiles $(u(x),v(x))$ for the PSS solutions are shown as insets. The letters CP, SN, and DP indicate circle-pitchfork, saddle-node, and drift-pitchfork bifurcations. The bifurcations delimit sections of the PSS solution branch: each section is labeled by its instability index, i.e., the number of (linearly indepen-

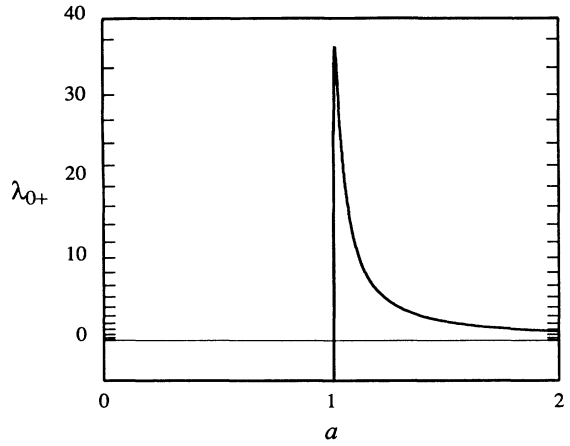

FIG. 4. Leading eigenvalue, λ_{0+}, of the middle-branch steady state. The eigenvalue crosses zero at $a=1+b=1.01$, corresponding to the transcritical bifurcation in Fig. 3. Growth rates of nonzero wave-number perturbations can be inferred from this figure via $\lambda_{k+}=\lambda_{0+}-(2\pi k/L)^2$. The periodic steady-state branch shown in Fig. 5 originates from $k=1$ circle-pitchfork bifurcations at $a=1.0101$ (see also Fig. 3), and at $a=17.71$ (not shown). The middle branch undergoes numerous other circle-pitchfork bifurcation with successively higher $k\leq 20$. Tick marks are at values $\lambda=(2\pi k/L)^2$ for $L=21.58$ and k integer.

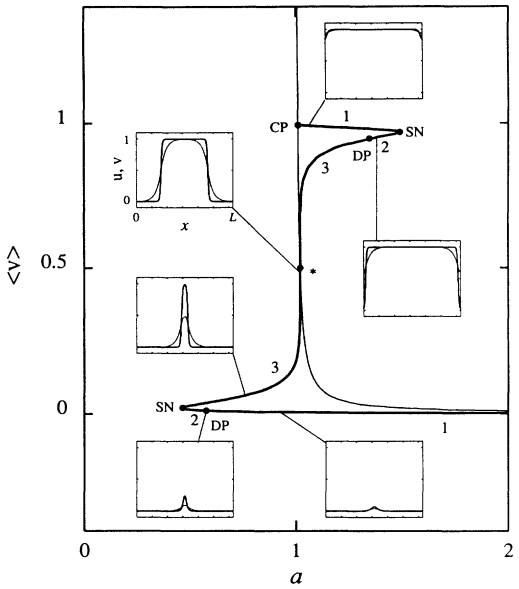

FIG. 5. Bifurcation diagram for periodic steady states (PSS). The spatial average $\langle v\rangle$ is plotted as a function of a. The thin curve shows the homogeneous middle branch $u=v=b/(a-1)$, from which the PSS solutions bifurcate. Dots indicate bifurcation points: circle pitchfork, CP; saddle node, SN; drift pitchfork, DP. With decreasing $\langle v\rangle$, bifurcations occur at $a=1.0101$ (CP), $a=1.489$ (SN), $a=1.346$ (DP), $a=0.464$ (SN), and $a=0.576$ (DP), and $a=17.71$ (CP; not shown). Numbers label the number of unstable eigenvalues. Insets are spatial profiles of u (thick) and v (thin) at (clockwise from lower right) $a=0.92$, 0.58, 0.76, 1.02, 1.38, and 1.06. The pulse branch shadows the middle branch: the profiles resemble $u=v=1$ near the first CP bifurcation and resemble $u=v=0$ near the second CP bifurcation. The parameter value $a=1+2b=1.20$ at which u and v have shift-and-reflect symmetry is indicated by an asterisk.

dent) eigenvectors to which a solution is unstable.

At $a=1.0101$ there is the circle-pitchfork bifurcation, through which the PSS branch arises from the HSS middle branch. A "circle" of PSS solutions is created from the pair of bifurcating eigenvectors $\tilde{\mathbf{u}}_0\cos(2\pi x/L)$ and $\tilde{\mathbf{u}}_0\sin(2\pi x/L)$. Each inset in Fig. 5 actually shows one member of such a circle of solutions. The PSS solutions are not invariant under rotation; instead, rotations $R(\alpha)$ transform PSS solutions into other PSS solutions. This implies the existence for each PSS solution $\mathbf{u}(x)$ of a marginal mode $d\mathbf{u}/dx$, with zero eigenvalue [as can be verified by substitution into (16) and (15)]. This marginal eigenvector "points" along the circle of solutions, and is a feature of all of the PSS and traveling-wave solutions. (The corresponding mode for the normal form is the θ unit vector.) Because the marginal mode is always present, the Jacobian at any steady-state bifurcation has two zero eigenvalues, rather than one. Marginal eigenvectors for two different PSS solutions are illustrated in Figs. 6(a) and 6(c). Like the steady states (5) in the normal form [Fig. 1(b)], each PSS solution has an axis of reflection symmetry. Consequently, all eigenvectors along this branch are either reflection symmetric or reflection antisymmetric, as can be seen in Figs. 6(a)–6(d).

Close to CP, the inset shows that PSS solutions resemble the one branch, with a slight depression that deepens as we move along the branch in the direction of increasing a. The middle branch is unstable prior to the CP bifurcation, and hence, the PSS branch inherits from the middle branch an instability index of 1. At $a=1.489$ there is a saddle-node bifurcation of the PSS branch which increases the instability index from 1 to 2. As we continue along the branch, now in the direction of decreasing a, we encounter the drift-pitchfork bifurcation at $a=1.346$ which increases the instability index of the PSS branch to 3. At DP, the Jacobian contains a Jordan block: the bifurcating eigenvector coalesces with the rotational mode $d\mathbf{u}/dx$. The drift pitchfork is responsible for the creation of the traveling-wave branch, and will be discussed in Sec. IV C.

As we continue along the PSS branch, the depression in the u and v profiles continues to deepen and widen, causing the average value $\langle v\rangle$ to decrease drastically. There exist two small intervals throughout which two of the three unstable eigenvalues form a complex conjugate pair. As discussed in Sec. III C, at the parameter value $a=1+2b$, Eq. (11) is invariant under the transformation $\mathbf{u}\rightarrow 1-\mathbf{u}$. This causes the PSS solutions to possess an additional symmetry sometimes referred to as shift-and-reflect $1-\mathbf{u}(x+L/2)=\mathbf{u}(x)$. Two eigenvectors at this parameter value are shown in Figs. 6(a) and 6(b).

We encounter a second saddle-node bifurcation at $a=0.464$ and a second drift-pitchfork bifurcation at $a=0.576$, which successively decrease the instability index from 3 to 2 and then to 1. The DP is a termination

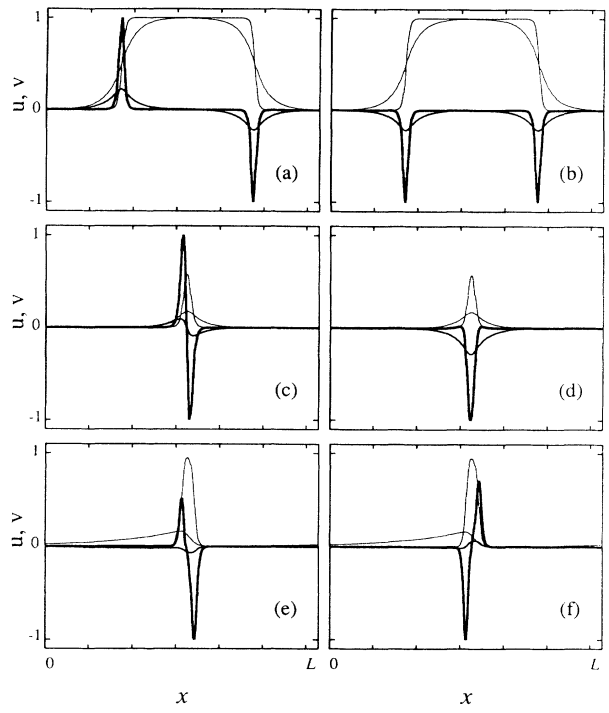

FIG. 6. Representative eigenvectors. The thin curves are the underlying periodic or traveling-wave states $\mathbf{u}=(u,v)$; the thick curves are the eigenvectors $\tilde{\mathbf{u}}=(\tilde{u},\tilde{v})$ whose eigenvalues are closest to zero. (a) and (b) are antisymmetric and symmetric eigenfunctions, respectively, for the periodic steady state which has shift-and-reflect symmetry at $a=1+2b=1.02$ in Fig. 5. (c) and (d) are eigenfunctions for the periodic state at the drift-pitchfork bifurcation at $a=0.464$. (c) is the antisymmetric marginal rotational mode $d\mathbf{u}/dx$ which has coalesced with another eigenvector to form a Jordan block. (d) is the symmetric eigenfunction which bifurcates at a nearby saddle node. (e) and (f) are the real and imaginary parts of a complex eigenvector for a traveling wave at $a=0.217$. These are associated with the nearby Hopf bifurcation in Fig. 7.

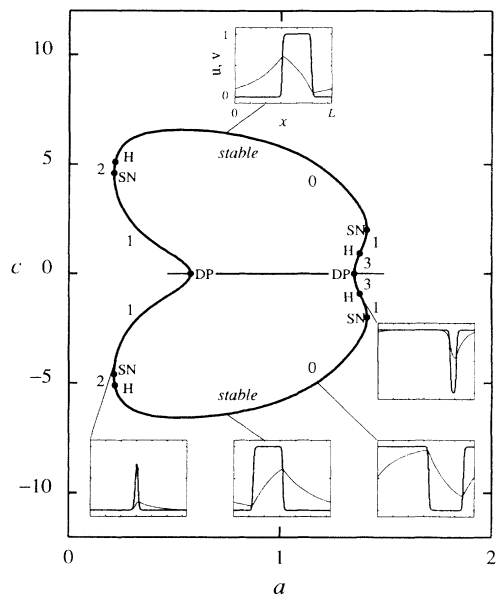

FIG. 7. Bifurcation diagram for traveling waves. The wave speed c is plotted as a function of a. The thin line at $c=0$ represents the periodic steady-state branch, and the thick curves represent the bifurcating branches of traveling waves. Dots indicate bifurcation points: drift pitchfork, DP; Hopf, H; and saddlenode, SN. Bifurcations occur at $a=1.347$ (DP), $a=1.374$ (H), $a=1.408$ (SN), $a=0.218$ (H), $a=0.213$ (SN), and $a=0.576$ (DP). Numbers label the number of unstable eigenvalues. Insets are spatial profiles of u (thick) and v (thin) at (counterclockwise from lower left) $a=0.24$, 0.75, 1.17, 1.38, and 0.75. Note that the bifurcation diagram is symmetric about $c=0$, and that the profiles of right-going waves are reflections of the left-going waves. Stable traveling waves exist over the interval $0.218<a<1.408$.

point for the traveling-wave branch. The eigenvectors associated with these two bifurcations are shown in Figs. 6(c) and 6(d). It can be seen that the eigenvector which bifurcates at SN [Fig. 6(c)] is reflection symmetric, whereas the bifurcating eigenvector at DP [Fig. 6(d)] is antisymmetric and identical to the translational mode $d\mathbf{u}/dx$.

The PSS has become quite narrow and it now begins to shorten as well. At $a=17.715$ (not shown in Fig. 5), the PSS branch terminates, via another circle pitchfork, on the homogenous middle branch.

C. Traveling waves

Shown in Fig. 7 is a bifurcation diagram for the traveling-wave solutions. Here we characterize each state by its wave speed c. As in Fig. 5, representative spatial profiles, $(u(x),v(x))$, are shown as insets. The bifurcations are indicated as before with H abbreviating Hopf bifurcation. The instability index of a traveling wave with wave speed c is calculated in a frame moving with velocity c according to (16), and is given by the number along the branch.

The traveling-wave branch arises from the PSS branch via drift-pitchfork bifurcations, analogous to that presented in Sec. II. At these bifurcation points, c, which corresponds to z in the normal form (1), is zero and the spatial profiles u and v are reflection symmetric. The drift pitchfork breaks the reflection symmetry and gives rise to two branches of traveling waves, one right-going ($c>0$) and one left-going ($c<0$), which are interchanged by reflection in x, as illustrated by the upper and lower insets at $a=0.75$.

Beginning our tour around Fig. 7 at the DP at $a=1.347$, following either the left- or right-going waves, we note that the traveling-wave branch inherits three unstable eigenvalues from the PSS branch. Two of these form a complex conjugate pair which undergoes a Hopf bifurcation H at $a=1.374$. The Hopf bifurcation decreases the instability index to 1 and creates a pair of unstable tori, i.e., modulated traveling waves. (We have not computed these unstable tori and they are not shown in the figure). The last remaining unstable eigenvalue

changes sign at the saddle-node bifurcation at $a=1.408$.

This, then, completes the sequence of bifurcations leading to the formation of stable traveling waves. They exist over the interval $0.218<a<1.408$. Thus the stable portion of the traveling-wave branch extends well into the excitable regime of the system $a<1+b=1.01$ (see Fig. 2).

The spatial profiles of the traveling waves follow the same qualitative trend as those along the underlying PSS branch. For $a\approx 1.4$, u and v are near one, with a narrow depression. This depression grows until, for $a\approx 0.2$, u and v are near zero, with a small spike. The difference between the leading and trailing edges of the v profile is more marked than that of the u profile, and the asymmetry grows with $|c|$.

At the low-a end of the bifurcation diagram, two bifurcations occur in rapid succession: a Hopf bifurcation at $a=0.218$ followed by a saddle-node bifurcation at $a=0.213$. The real and imaginary parts of the bifurcating eigenvectors at H are shown in Figs. 6(e) and 6(f). The complex eigenvalues at H become real as a is decreased and one of these eigenvalues goes to zero at SN. Hence the H and SN bifurcations are probably associated with the unfolding of a double-zero bifurcation [48]. If this is the case, then the unstable tori created at the Hopf bifurcation disappear via a global saddle-loop bifurcation, by colliding with the singly unstable portion of the traveling-wave branch close to the SN. Finally, the traveling-wave branch is reabsorbed into the PSS branch by a second drift pitchfork at $a=0.576$.

V. DISCUSSION AND CONCLUSION

We have computed bifurcation diagrams for spatially homogeneous steady states, spatially periodic steady states, and periodic traveling waves along a particular one-parameter path of a model excitable medium. In so doing, we have shown how traveling wave states are connected via symmetry-breaking bifurcations to a fully symmetric, homogeneous steady state. The middle-branch steady state, which gives rise to the periodic steady states and traveling waves, is itself connected to the excitable zero branch in a (nonsymmetry-breaking) transcritical bifurcation along the curve $b=0$ (Fig. 2). Thus we have clearly identified the bifurcations which connect the two most basic states of an excitable medium: the homogeneous excitable state and stable traveling waves.

We have not attempted a comprehensive investigation of parameter space. Except for the homogeneous steady states, we have not considered the effect of varying the kinetic parameters ϵ and b. More importantly, we have kept the length L fixed, and so have followed only one branch of a continuum of solutions parametrized by L. We have been content to keep these parameters fixed because much is already known about traveling waves in excitable media [1]–[17]. Our purpose has been instead to focus explicitly on the various symmetry-breaking bifurcations occurring in the system.

We conclude by mentioning the overlap between the results presented here and other studies of reaction-diffusion systems. In particular, Dockery and Keener [12], and McCarty and Horsthemke [13] have computed drift-pitchfork bifurcations to traveling waves in other models or excitable media, though they did not identify the symmetry breakings associated with these bifurcations. Farr and Golubitsky [18] have considered in detail Hopf bifurcations with O(2) symmetry for the Gray-Scott model. While the Gray-Scott model is not a model of excitability, the results of Farr and Golubitsky might apply to excitable systems. For instance, outside the excitability regime the model we have studied undergoes homogeneous Hopf bifurcations (region IV of Fig. 2). Hence we expect there to be O(2)-symmetric Hopf bifurcations in region IV. We have not explored this, however, and we do not know whether there are traveling-wave branches originating in region IV which stabilize in the excitable regime. We leave this for future work.

ACKNOWLEDGMENTS

M. K. and L.S.T. have been supported by NSF Grant Nos. DMS-8901767 and DMS-9113142, by NSF Undergraduate Research Supplement, and by a University of Texas URI Research Grant.

[1] A. T. Winfree, *When Time Breaks Down* (Princeton University Press, Princeton, NJ, 1987).
[2] V. S. Zykov, *Modelling of Wave Processses in Excitable Media* (Manchester University Press, Manchester, 1988).
[3] J. J. Tyson and J. P. Keener, Physica D **32**, 327 (1988).
[4] Waves and Patterns in Chemical and Biological Media, edited by H. L. Swinney and V.I. Krinsky, Physica D **49** (1991).
[5] Th. Erneux and M. Herschkowitz-Kaufman, J. Chem. Phys. **66**, 248 (1977).
[6] R. N. Miller and J. Rinzel, Biophys. J. **34**, 227 (1981).
[7] P. C. Fife, J. Stat. Phys. **39**, 687 (1985).
[8] K. Maginu, SIAM J. Appl. Math. **45**, 750 (1985).
[9] Z. Noszticzius, W. Horsthemke, W. D. McCormick, H. L. Swinney, and W. Y. Tam, Nature (London) **329**, 619 (1987).
[10] J. D. Dockery, J. P. Keener, and J. J. Tyson, Physica D **30**, 177 (1988).
[11] A. Pagola, J. Ross, and C. Vidal, J. Phys. Chem. **92**, 163 (1988).
[12] J. D. Dockery and J. P. Keener, SIAM J. Appl. Math. **49**, 539 (1989).
[13] P. McCarty and W. Horsthemke, J. Chem. Phys. **91**, 5597 (1989).
[14] P. Foerster, S. C. Müller, and B. Hess, Proc. Natl. Acad. Sci. USA **86**, 6831 (1989).
[15] H. Sevcikova and M. Marek, Physica D **39**, 15 (1989).
[16] C. Elphick, E. Meron, and E. A. Spiegel, SIAM J. Appl. Math. **50**, 490 (1990).
[17] D. A. Kessler and H. Levine, Phys. Rev. A **41**, 5418 (1990).
[18] W. W. Farr and M. Golubitsky, SIAM J. Appl. Math. **52**,

181 (1992).
[19] D. Barkley, M. Kness, and L. S. Tuckerman, Phys. Rev. A **42**, 2489 (1990).
[20] D. Barkley, Physica D **49**, 61 (1991).
[21] B. A. Malomed and M. I. Tribelsky, Physica D **14**, 67 (1984).
[22] O. Thual and C. Bellevaux, in Current Trends in Turbulence Research, edited by H. Branover, M. Mond, and Y. Unger [Prog. Astron. Aero. **112**, 332 (1988)].
[23] D. Armbruster, J. Guckenheimer, and P. Holmes, Physica D **29**, 257 (1988).
[24] A. J. Simon, J. Bechhoefer, and A. Libchaber, Phys. Rev. Lett. **61**, 2574 (1988).
[25] G. Faivre, S. de Cheveigné, C. Guthmann, and P. Kurowski, Europhys. Lett. **9**, 779 (1989).
[26] I. G. Kevrekidis, B. Nicolaenko, and J. C. Scovel, SIAM J. Appl. Math. **50**, 760 (1990).
[27] P. Coullet and G. Iooss, Phys. Rev. Lett. **64**, 866 (1990).
[28] W. J. Rappel and H. Riecke, Phys. Rev. A **45**, 846 (1992).
[29] B. Caroli, C. Caroli, and S. Fauve, J. Phys. (Paris) I **2**, 281 (1992).
[30] M. R. E. Proctor and C. A. Jones, J. Fluid Mech. **188**, 301 (1988).
[31] S. Douady, S. Fauve, and O. Thual, Europhys. Lett. **10**, 309 (1989).
[32] P. Coullet, R. E. Goldstein, and G. H. Gunaratne, Phys. Rev. Lett. **63**, 1954 (1989).
[33] M. Rabaud, S. Michalland, and Y. Couder, Phys. Rev. Lett. **64**, 184 (1990).
[34] S. Fauve, S. Douady, and O. Thual, J. Phys. (Paris) II **1**, 311 (1991).
[35] H. Riecke, Phys. Rev. A **45**, 8605 (1992).
[36] M. Golubitsky, I. Stewart, and D. G. Schaeffer, *Singularities and Groups in Bifurcation Theory* (Springer, New York, 1988), Vol. II.
[37] J. D. Crawford and E. Knobloch, Annu. Rev. Fluid Mech. **23**, 341 (1991).
[38] G. D. Smith, *Numerical Solution of Partial Differential Equations: Finite Difference Methods* (Clarendon, Oxford, 1985).
[39] W. H. Press, B. P. Flannery, S. A. Teukosky, and W. T. Vetterling, *Numerical Recipes: the Art of Scientific Computing* (Cambridge University Press, Cambridge, England, 1988).
[40] M. Kubíček and M. Marek, *Computational Methods in Bifurcation Theory and Dissipative Structures* (Springer, New York, 1983).
[41] R. Seydel, *From Equilibrium to Chaos: Practical Bifurcation and Stability Analysis* (Elsevier, New York, 1988).
[42] D. Sorensen, SIAM J. Matrix Analysis and Applications **13**, 357 (1992).
[43] W. S. Edwards, L. S. Tuckerman, R. A. Friesner, and D. Sorensen, J. Comput. Phys. (to be published).
[44] A. Karma, Phys. Rev. Lett. **68**, 397 (1992); J. P. Keener, SIAM J. Appl. Math. **52**, 1370 (1992).
[45] The model kinetics have been designed for fast time stepping [19,20] and this necessitates a u nullcline with unphysical branches indicated with dashed lines in Fig. 2.
[46] P. DeKepper and J. Boissonade, in *Oscillations and Traveling Waves in Chemical Systems,* edited by R. J. Field and M. Burger (Wiley, New York, 1985).
[47] Corners in the u nullcline give rise to transcritical steady-state bifurcations. In generic models, the u nullcline is smooth and correspondingly the steady-state bifurcations are saddle nodes. It is unlikely, however, that the difference between the transcritical bifurcations here and the more generic saddle nodes is of any consequence.
[48] J. Guckehheimer and P. Holmes, *Nonlinear Oscillations, Dynamical Systems, and Bifurcations of Vector Fields* (Springer, New York, 1983).